Numerical investigation of oblique detonation structure in hydrogen-oxygen mixtures with Ar dilution

Cheng Tian[1], Honghui Teng[1,*], and Hoi Dick Ng[2]

(1. School of Aerospace Engineering, Beijing Institute of Technology, Beijing 100081, China;

2. Department of Mechanical, Industrial and Aerospace Engineering, Concordia University, Montreal, QC, H3G 1M8, Canada)

Abstract: Two combustible mixtures, H_2-O_2-Ar and H_2-O_2-N_2, are widely used in detonation research, but only the latter has been employed in oblique detonation wave (ODW) studies. In this study, ODWs in H_2-O_2-Ar are simulated to investigate their structural characteristics using reactive Euler equations with a detailed chemistry model. Similar to ODWs in H_2-O_2-N_2 mixtures, two observed structures are dependent on incident Mach numbers. However, in mixtures of $2H_2+O_2+7Ar$, the structures are sensitive to inflow static pressure P_0, different from the structures in H_2-O_2-N_2 mixtures. Based on flow field analysis, the ratio of induction and heat release zone lengths R_L is proposed to model the difference induced by dilution gas. Generally, R_L is large in N_2 diluted mixtures but small in Ar diluted mixtures. Low R_L indicates that induction is comparable with the heat release zone and easily changed, resulting in pressure-sensitive structures. When the dilution gas changes gradually from N_2 to Ar, the ratio R_L increases slowly at first and then declines rapidly to approach a constant. The variation rule of R_L is analyzed and compared with results from calculations of a constant volume explosion, demonstrating how different dilution gases influence ODW structures.

Key words: oblique detonation, hydrogen, wave structure

* Corresponding author.
E-mail address: hhteng@bit.edu.cn (H. Teng).

1. Introduction

Premixed combustible mixtures contain two kinds of combustion waves, detonation and deflagration waves [1]. Detonation waves propagate at a supersonic speed, achieving self-ignition combustion behind the leading shock. Due to compression of the leading shock, successive combustion achieves high thermal efficiency as a form of pressure-gain combustion. Therefore, replacing deflagration with detonation in engines may benefit the propulsion system from a theoretical perspective. Recently, detonation-based combustion has attracted increasing attention due to its potential use in aeronautics and astronautics propulsion [2-5].

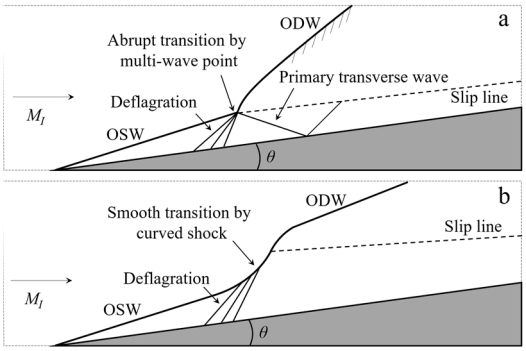

Fig. 1 Sketch of ODW structures: (a) abrupt transition and (b) and smooth transition.

The oblique detonation engine, also called a shock-induced combustion ramjet, is a propulsion device based on the oblique detonation wave (ODW). To facilitate application, fundamental studies on ODWs have been performed to understand underlying coupling of the oblique shock wave (OSW) and heat release. In early studies (e.g., [6]), ODW structures were usually simplified as an OSW coupled with an instant post-shock heat release. However, later studies [7-11] demonstrated that the ODW surface is composed of a non-reactive OSW before an oblique detonation surface forms. Two detailed ODW structures exist as shown in Fig. 1. One is an abrupt transition, featuring a multi-wave point, and the other is a smooth transition featuring curved shock. Besides wave morphology, several studies have focused on local structures on ODW surfaces, illustrating the formation and evolution of fine-scale features [12-18].

Detonation waves have a few dynamic parameters, such as cell width, determined

by the properties of combustible mixtures. Various mixtures have been studied on normal detonations [19-23] and rotating detonations [24,25], demonstrating different wave behaviors. Nevertheless, most previous ODW studies were based on the one-step irreversible heat release model, in which chemical reactions are undoubtedly oversimplified. A two-step induction-reaction chemistry model has been considered to study ODW initiation and surface instability [26,27], demonstrating novel phenomena. Detailed chemical reaction models are helpful when studying different fuels, although come at the cost of complex and expensive chemical kinetic computations. Recently, several numerical studies were performed using chemical reaction models, examining the effects of inflow inhomogeneity [28,29] and the initiation mechanism [30,31] to illustrate ODW characteristics in H_2-air (i.e., H_2-O_2-N_2) mixtures.

In this study, H_2-O_2 mixtures with Ar dilution are used to study the ODW structure. This mixture has been widely used in detonation physics studies (e.g., [32-34]), mainly because it is relatively stable so that the cellular detonation structure is highly regular. The present numerical results reveal that the ODW structures in H_2-O_2-Ar mixtures are sensitive to inflow static pressure, different those in H_2-O_2-N_2 mixtures and never been reported before. Based on serial simulations, the ratio of induction and heat release zone lengths is proposed to model the difference, and how different dilution gases influence ODW structures is also discussed.

2. Physical and mathematical models

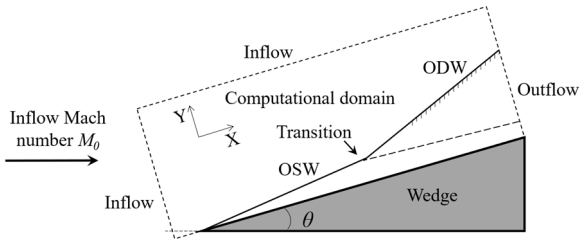

Fig. 2 Sketch of wedge-induced oblique detonation simulation.

Following our previous studies (e.g., [27,30]), a schematic of typical ODWs induced by a two-dimensional, semi-infinite wedge is given in Fig. 2. The presence of the wedge in a supersonic combustible inflow first induces an OSW. For a high inflow Mach

number causing a high post-shock temperature behind the OSW, an exothermic chemical reaction begins, leading to ODW formation. The coordinate is rotated to the direction along the wedge surface, and the Cartesian grid in the rectangular domain enclosed by the dashed line in Fig. 2 is aligned with the wedge surface. Ignoring the viscosity and diffusion effects, the governing equations are unsteady reactive Euler equations:

$$\frac{\partial \mathbf{U}}{\partial t}+\frac{\partial \mathbf{F}}{\partial x}+\frac{\partial \mathbf{G}}{\partial y}=\mathbf{S} \tag{1}$$

where

$$\mathbf{U}=\begin{Bmatrix}\rho_1\\ \vdots\\ \rho_n\\ \rho u\\ \rho v\\ e\end{Bmatrix},\ \mathbf{F}=\begin{Bmatrix}\rho_1 u\\ \vdots\\ \rho_n u\\ \rho u^2+p\\ \rho uv\\ (e+p)u\end{Bmatrix},\ \mathbf{G}=\begin{Bmatrix}\rho_1 v\\ \vdots\\ \rho_n v\\ \rho uv\\ \rho v^2+p\\ (e+p)v\end{Bmatrix},\ \mathbf{S}=\begin{Bmatrix}\omega_1\\ \vdots\\ \omega_n\\ 0\\ 0\\ 0\end{Bmatrix} \tag{2}$$

The total density and total energy are calculated by

$$\rho=\sum_{i=1}^{n}\rho_i\ ,\quad e=\rho h-p+\frac{1}{2}\rho\left(u^2+v^2\right) \tag{3}$$

where specific enthalpy can be written as $h=\sum_{i=1}^{n}\rho_i h_i/\rho$ with h_i obtained from the thermodynamic data of each individual specie. The state equation is

$$p=\sum_{i=1}^{n}\rho_i\frac{R_0}{w_i}T \tag{4}$$

where w_i is the molecular weight; T is the gas temperature; and ω_i is the species' specific mass production rate, which is determined by the chemical reaction model.

The chemical kinetic model used in this study is taken from a comprehensive H_2/O_2 kinetic model for high-pressure combustion [35]. This mechanism involves 27 reversible, elementary reactions among 8 species (H_2, O_2, H_2O, H, O, OH, and HO_2 and H_2O_2) with 5 inert species (N_2, Ar, He, CO, and CO_2). Thermodynamic properties of the chemical species are evaluated using the 9-coefficient NASA polynomial representation [36]. The governing equations are discretized on Cartesian uniform grids

and solved with the DCD scheme [37] with Strang's splitting. To overcome the stiff problem, a sufficient number of sub-reaction steps are involved to ensure overall accuracy [38].

Unless specified, $2H_2+O_2+7Ar$ is used as the default stoichiometric mixture with wedge angle 25º. In this study, the inflow temperature is 298.15 K for all cases, while the inflow static pressure P_0 varies as an important parameter. In all figures, the dimensions of temperature, pressure, and density are K, Pa, and kg/m^3, respectively. The incident Mach number M_0 changes between 6.5–8.0, and in most cases M_0 = 7.0. The slip reflecting boundary condition is used on the wedge surface, and other boundaries are interpolated under the assumption of zero first-order derivatives of all flow parameters. On the lower computational boundary, the wedge starts from x = 0.512 mm. Initially, all flow fields are uniform, and the simulation does not stop until the flow fields reach a steady state. Due to the multi-scale nature of the phenomena, the computational domain and mesh scale are each adjusted, and resolution studies are conducted to ensure grid-independence of global characteristic features.

3. Numerical results and discussion

3.1 Effects of M_0 on the ODW structure

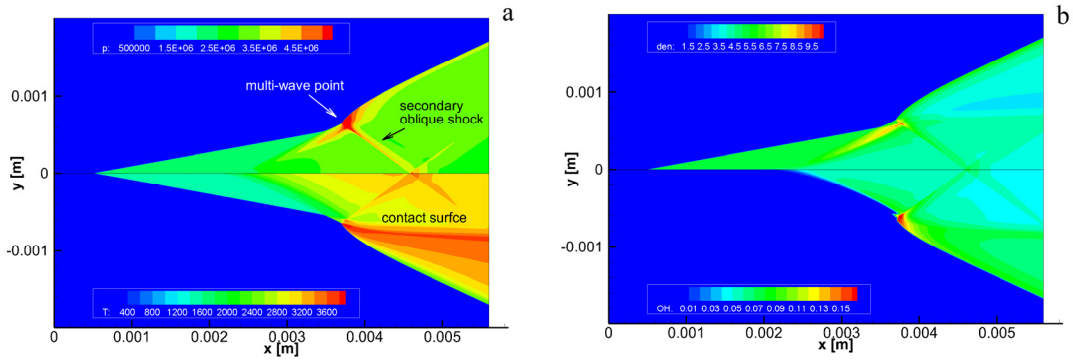

Fig. 3 Pressure, temperature, density and OH density with M_0 = 7, P_0 = 1.0 atm.

ODW with M_0 = 7 and P_0 = 1.0 atm is simulated first and shown in Fig. 3. The oblique surface is composed of two sections, an inert shock upstream and a detonation surface downstream. Two sections are connected by a multi-wave point, displaying a

typical abrupt transition structure. From the multi-wave point, the secondary oblique shock and contact surface (slip line) extend downstream in the combustion product. The secondary oblique shock can be observed clearly in the temperature field, as it reflects on the wedge and generates a local high-temperature region there. The contact surface is almost parallel with the surface, and different temperature values can be observed. A contact surface that extends downstream from the multi-wave point forms due to different waves. On the near-wedge side, heat release is achieved by deflagration, whereas heat release is achieved by detonation on the other side, resulting in different temperature.

A resolution study was performed on the structure in Fig. 3, and the results and relevant discussion are provided in Appendix A. Generally, the grid size of 4 μm used in Fig. 3 is deemed sufficient to capture main flow characteristics, and refining it to 2 μm results in the same flow fields. For other cases shown later, similar resolution studies were performed to assess and avoid the effects of grid scales.

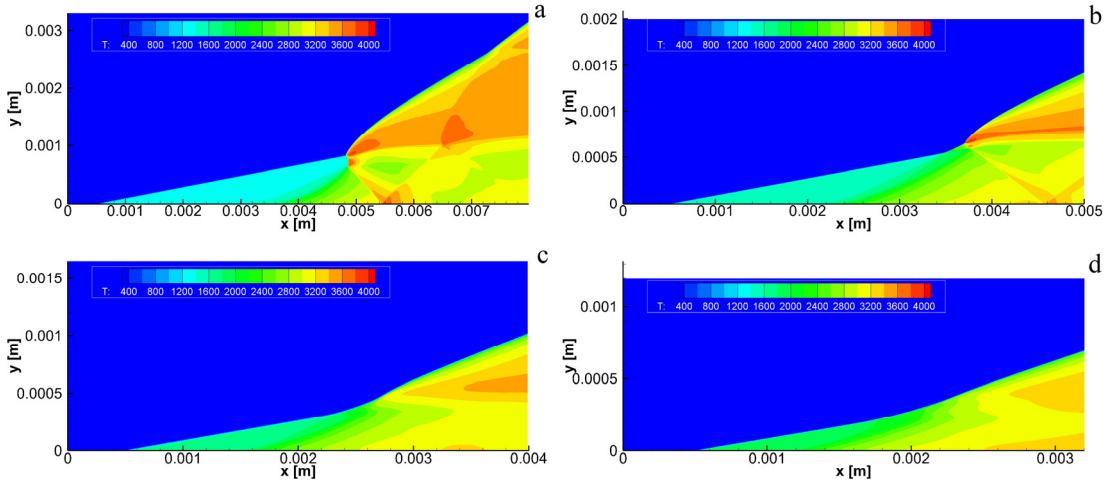

Fig. 4 Temperature fields in the cases of P_0 = 1.0 atm and M_0 = 6.5 (a), 7.0 (b), 7.5 (c), 8.0 (d)

ODWs with different M_0 were simulated and are shown in Fig. 4. A previous study with N_2 dilution [30] provided results with M_0 = 7.0–10.0, enabling structural variation to be distinguished. Nevertheless, given the same M_0, ODW in Ar dilution mixtures has a high post-shock temperature; as such, relatively low Mach numbers are used, and structural variation dependent on M_0 can be observed. Figure 4 illustrates that wave structures are sensitive to M_0, and the initiation length changes substantially. In the case

of M_0 = 6.5, the structure features an abrupt transition, secondary oblique shock, and contact surface, similar to that shown in Fig. 3a but more complicated. Due to low M_0, one short Mach stem forms beneath the multi-wave point, and the secondary oblique shock becomes relatively strong; its wedge reflection and successive interaction with the contact surface are clear. By increasing M_0, the structure changes from an abrupt transition (Figs. 4a and 4b) into a smooth transition (Figs. 4c and 4d). Correspondingly, the oblique shock and contact surface become weaker and disappear gradually. These results are qualitatively identical to those in previous studies [10,15] despite the use of different chemical reaction models.

3.2 Effects of P_0 on the ODW structure

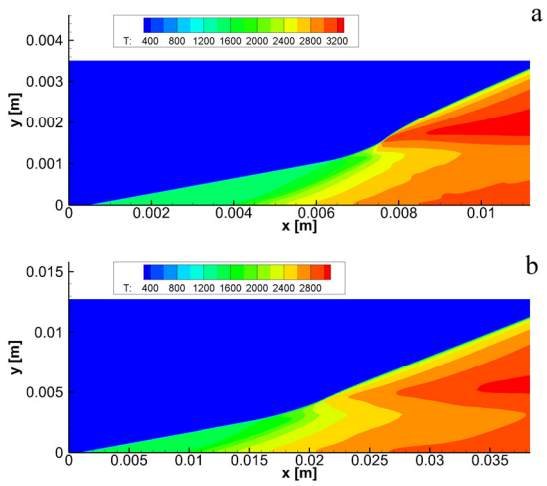

Fig. 5 Temperature fields in the cases of M_0 = 7.0: (a) P_0 = 0.5 atm and (b) 0.2 atm.

ODWs with P_0 = 0.5 and 0.2 atm are simulated to examine the effects of P_0 with results shown in Fig. 5. The wave structures are also sensitive to P_0, similar to the effects of M_0. With relatively high P_0, the structure tends to exhibit an abrupt transition, and declining P_0 results in a smooth transition as displayed in Fig. 5. The smooth structure is simpler than the abrupt structure given the lack of secondary oblique shock and contact surface. Generally, the effects of declining P_0 are similar to those of increasing M_0, so the results of Fig. 4d and Fig. 5b are comparable, but the initiation length of Fig. 5b is roughly ten times that of Fig. 4c.

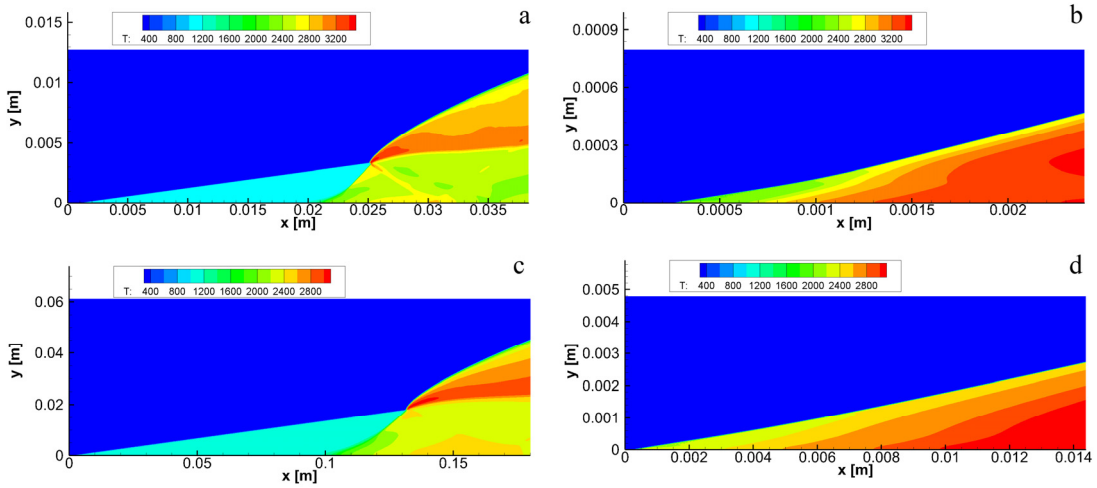

Fig. 6 Temperature fields in the mixtures of $2H_2+O_2+7N_2$: (a) $M_0 = 7.0$, $P_0 = 1.0$ atm; (b) $M_0 = 9.0$, $P_0 = 1.0$ atm; (c) $M_0 = 7.0$, $P_0 = 0.2$ atm; (d) $M_0 = 9.0$, $P_0 = 0.2$ atm.

Although P_0 is an important parameter in ODW formation, most previous studies only examined the effects of M_0. The reason may be due to wide use of the one-step kinetic model, in which the effects of P_0 cannot be elucidated directly. Our recent study [30] addressed the effects of P_0 in stoichiometric H_2-air mixtures, concluding that those structures are not sensitive to P_0, different from the results in Fig. 5. Considering that both studies used the same set of codes, including the same shock-capturing scheme and detailed chemistry model [35], the difference should be derived from the combustion characteristics of mixtures. The previous study [30] used a mixture of $2H_2+O_2+3.76N_2$, and additional simulations were performed with mixtures of $2H_2+O_2+7N_2$ to confirm and possibly exclude effects of the N_2 dilution ratio. Figure 6 presents numerical results in the cases of $M_0 = 7$ and 9 with different P_0. Obviously, the structures vary when M_0 changes, but they are not sensitive to P_0. Declining P_0 will not change the transition type from OSW to ODW, namely the abrupt transition in the case of $M_0 = 7$ and the smooth transition in the case of $M_0 = 9$. Furthermore, similar wave configurations appear independent of P_0, as shown in Figs. 6a and 6c or Figs. 6b and 6d. Therefore, whether the structure is sensitive to P_0 is determined by the dilution gas, that is, the structure is sensitive to P_0 in H_2-O_2-Ar mixtures but not in H_2-O_2-N_2 mixtures.

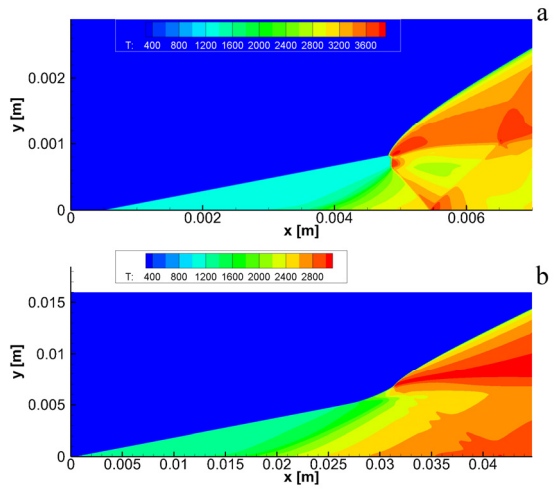

Fig. 7 Temperature fields in the cases of M_0 = 6.5: (a) P_0 = 1.0 atm and (b) 0.2 atm.

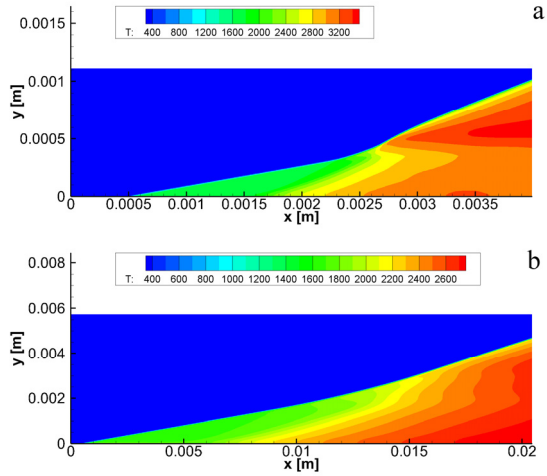

Fig. 8 Temperature fields in the cases of M_0 = 7.5: (a) P_0 = 1.0 atm and (b) 0.2 atm

To verify whether the effects of P_0 are universal, further simulations with M_0 = 6.5 and 7.5 were performed with results displayed in Figs. 7 and 8. The structures may be abrupt or smooth in the case of M_0 = 6.5, depending on P_0, similar to cases of M_0 = 7.0. When M_0 = 7.5, both structures are smooth but demonstrate notable differences. The oblique angle rising from OSW to ODW is obvious with high P_0, whereas only a slight rise is generated with low P_0. Therefore, structural sensitivity to P_0 appears to be a universal phenomenon in H_2-O_2-Ar mixtures regardless of M_0.

3.3 Analysis of structural characteristics

Interestingly, the ODW structure is sensitive to M_0 and P_0 in the H_2-O_2-Ar mixtures, but further analysis is difficult. With a one- or two-step global kinetics model,

simulations are usually performed by changing one parameter, such as activation energy, while keeping others the same. Nevertheless, no explicit bifurcation parameters can be controlled in detailed chemical reaction models; the corresponding chemical parameters of the entire system are calculated implicitly from many detailed chemical reactions, which are also controlled by the gas species and their fraction. In addition, analyzing these results becomes complex and requires more interpretation techniques.

To explore the underlying reason for various sensitivities, we first examine the corresponding M_{CJ} values, specifically the Mach number of the Chapman-Jouguet (CJ) detonation. Previous works [13,14] found that the structure depends on the overdriven degree f_{od}, defined by $(M_0 sin\beta/M_{CJ})^2$ in which β denotes the oblique detonation angle. When P_0 changes, the corresponding M_{CJ} changes as well, resulting in ODWs with different f_{od}, so ODWs may have different structures even with the same M_0. To examine whether this dominates structural variation, Table 1 lists the Mach numbers and velocities of CJ detonations with different mixtures. Obviously, M_{CJ} is larger in $2H_2+O_2+7Ar$ mixtures and smaller in $2H_2+O_2+7N_2$ mixtures. However, variations in M_{CJ} are limited for both mixtures (i.e., less than 3%). This limited variation of f_{od} does not strongly support structural sensitivity to P_0; therefore, it is necessary to explore other explanations for why ODW structures are sensitive to P_0 in H_2-O_2-7Ar mixtures.

Table 1 Mach numbers and velocities of CJ detonations.

P_0 (atm)	M_{CJ}		CJ velocity (m/s)	
	7Ar	$7N_2$	7Ar	$7N_2$
1.0	4.714	4.461	1693	1726
0.8	4.770	4.457	1687	1724
0.6	4.802	4.452	1679	1722
0.4	4.824	4.444	1668	1719
0.2	4.842	4.428	1648	1713

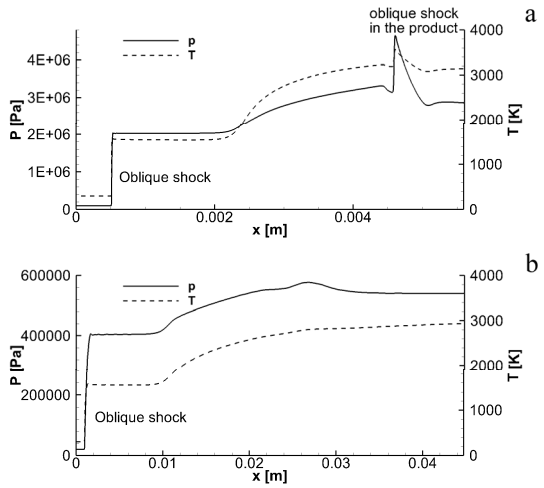

Fig. 9 Pressure and temperature along $y = 0$ in the cases of $M_0 = 7$: (a) $P_0 = 1.0$ atm and (b) 0.2 atm.

To analyze more fully the sensitivity, curves of pressure and temperature along $y = 0$ are shown in Fig. 9, in the cases of $M_0 = 7$ and $2H_2+O_2+7Ar$ mixtures. Due to different P_0, the post-oblique shock pressure of Fig. 9a is five times of that of Fig. 9b, and two frames have the same post-oblique shock temperature. However, deviations in temperature curves appear in the rising stages (i.e., the heat release zone). Overall, the increase is steeper in the case of $P_0 = 1.0$ atm and slow in the case of $P_0 = 0.2$ atm. In Fig. 9a, reaching 3000 K in the heat release zone brings the length close to that of the induction zone. Nevertheless, in the case of $P_0 = 0.2$ atm shown in Fig. 9b, the same temperature increase takes about 3 times its induction zone length. This difference may be responsible for structural sensitivity to P_0, which suggests the need to examine the heat release processes of ODW further.

To quantify the above analysis, two characteristic lengths, L_i and L_r, are defined as the induction zone length and heat release zone length, respectively. Neither a well-defined induction zone nor heat release zone pertains to the results of detailed chemistry models. Methods of defining L_i and L_r in this study are discussed in Appendix B. Numerical results indicate that with the same M_0 and P_0 (e.g., $M_0 = 7$, $P_0 = 1.0$ atm), heat release processes differ greatly in H_2-O_2-Ar and H_2-O_2-N_2 mixtures. The former mixture results in higher post-oblique shock temperature, and the heat release process starts easily but modestly. Contrarily, heat release is difficult to start but demonstrates a sharp profile in H_2-O_2-N_2 mixtures. Table 2 shows the length ratio R_L, defined by L_i/L_r,

as a function of M_0 and P_0 in both mixtures. ODWs in H_2-O_2-Ar mixtures have small R_L whereas those in H_2-O_2- N_2 mixtures have large R_L. In general, R_L serves as a good criterion to determine whether ODW structures are sensitive to P_0.

Table 2 R_L with different mixtures and M_0.

P_0 (atm)	M_0 = 6.5		M_0 = 7.0		M_0 = 7.5	
	7Ar	7N_2	7Ar	7N_2	7Ar	7N_2
1.0	4.76	53.3	3.49	24.4	3.17	17.1
0.8	3.86	43.3	3.33	22.4	2.75	14.1
0.6	3.31	42.7	2.55	22.2	2.13	12.5
0.4	2.41	38.9	1.96	20.4	1.57	11.4
0.2	1.41	28.7	1.22	15.0	1.06	8.16

Before analyzing why R_L varies so significantly, it should be noted that a similar parameter χ has been proposed to quantify the instability of normal detonations [39]. That study revealed that unstable detonations with irregular oscillation patterns and cellular structures generally have large χ values. Because the effects of activation energy have been considered there, the parameters R_L and χ cannot be compared directly. Drawing from the previous study [39], normal detonations with high R_L should be more unstable with irregular cellular structures and vice versa. That finding seems incongruent with the present study because ODW structures with high R_L seem more stable. The discrepancy is attributable to different definitions of instability and the role of the induction zone. For normal detonations, the relatively long induction zone and correspondingly high R_L favor the amplification of a disturbance and result in strong instability. For oblique detonations, the long induction zone is the post-oblique shock region in which the flow is supersonic. High R_L indicates that the induction is much longer than the heat release zone, so difficult to change via heat release processes. This induces stable structures independent of P_0. Therefore, this study on steady, oblique detonations does not oppose the previous study on unsteady, normal detonations [39].

3.4 Discussion of dilution effects

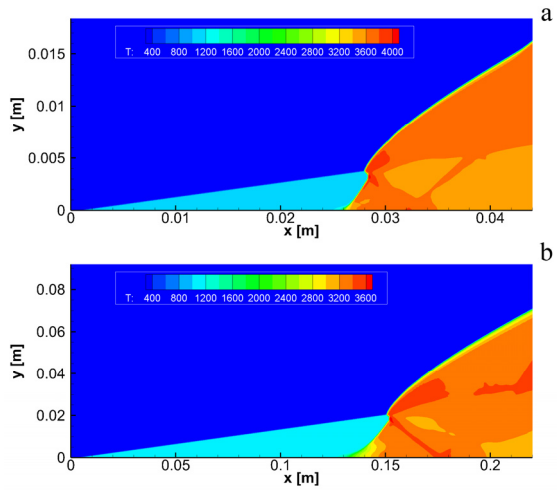

Fig. 10 Temperature fields in the cases of M_0 = 7.0: (a) P_0 = 0.3 atm and (b) 0.06 atm in $2H_2+O_2$ mixtures.

To analyze variation in R_L and extend the discussion on dilution gas effects, ODWs in $2H_2+O_2$ with no dilution were simulated. In previous cases with 70% dilution, either $2H_2+O_2+7Ar$ or $2H_2+O_2+7N_2$, the partial pressure of fuel and oxidant accounts for 30%; thus, two P_0 values, 0.3 atm and 0.06 atm, are chosen to maintain the same amount of $2H_2+O_2$. As shown in Fig. 10, the structure is not sensitive to P_0, demonstrating two similar abrupt structures in this kind of mixture. This pattern suggests that ODWs in undiluted $2H_2+O_2$ mixtures are similar to those in $2H_2+O_2+7N_2$ mixtures and not those in $2H_2+O_2+7Ar$ mixtures.

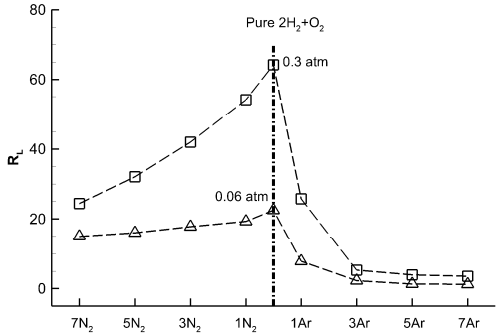

Fig. 11 R_L with different dilution ratio of Ar and N_2 dilution, keeping same amount of $2H_2+O_2$.

Following the idea of keeping the same amount of $2H_2+O_2$, more cases were

simulated with different dilution ratios (i.e., 10%, 30%, and 50%) in both mixtures. Figure 11 displays the length ratio R_L variation, whose maximum values appear in cases of no dilution. On the left branch, increasing N_2 dilution causes R_L to decline, which occurs more quickly in cases of high pressure. On the right branch, R_L declines with increasing Ar dilution, showing an exponential-like profile. R_L first declines rapidly from 0 Ar to 3 Ar and then approaches a constant asymptotically.

It is unsurprising that the variation in R_L depends on the dilution gas. Besides the reaction mechanism itself, whether other factors contribute to the R_L in ODW simulations should be clarified. A theoretical approach based on calculations of the constant volume explosion is used to obtain the theoretical R_L, assuming an ideal post-oblique shock flow, where pressure build-up in well-premixed mixtures and the formation of pressure waves are weak near the wedge. Under these assumptions, calculations were performed using the CHEMKIN package [40], and results following the definition in Appendix B were compared with numerical findings in Table 3. The theoretical results are not the same as the numerical findings, demonstrating that R_L is also influenced by the effects of gas dynamics rather than solely by chemical reactions. The theoretical and numerical results are relatively similar when the dilution gas is Ar, suggesting that the effects of chemical reactions play an important role in these cases. Similar to this work, the cell sizes in Ar dilution mixtures are predicted much more accurately than those in N_2 dilution mixtures, as indicated in research on numerical cell size with the same mechanisms [34]. Further investigation on the effects of gas dynamics and chemical reaction mechanisms are needed.

Table 3 Numerical and theoretical R_L with different mixtures and $M_0 = 7.0$.

	$P_0 = 0.3$ atm		$P_0 = 0.06$ atm	
	Numerical	Theoretical	Numerical	Theoretical
7Ar	3.49	4.45	1.22	1.82
5Ar	3.90	5.31	1.29	2.12
3Ar	5.24	8.76	2.28	3.79
Ar	25.78	48.69	7.82	12.06

No dilution	64.21	1472.78	22.53	38.96
N_2	54.17	2643.17	19.31	30.00
$3N_2$	41.95	4348.92	17.83	30.41
$5N_2$	32.10	Very high	16.03	29.91
$7N_2$	24.44	Very high	15.01	31.20

Table 4 L_i and L_r with different mixtures and M_0 = 7.0.

	P_0 = 0.3 atm		P_0 = 0.06 atm	
	L_i (mm)	L_r (mm)	L_i (mm)	L_r (mm)
7Ar	1.65	0.47	8.85	6.64
No dilution	24.8	0.39	126	5.58
$7N_2$	19.5	0.80	97.3	6.48

To elucidate the effects of different mixtures, Table 4 shows L_i and L_r with different mixtures and M_0 = 7.0. L_r changes a little, and the dominant variation of R_L should be attributed to the change of L_i. These results demonstrate how the type and amount of dilution gas change the combustion process of ODWs. Regarding the effects of dilution gas, two patterns are expected: accelerating chemical reactions through the third-body effects and changing the mixture properties. Due to third-body effects, L_i and L_r each decline but L_i varies more substantially regardless of the dilution gas, so that R_L declines when the dilution gas increases. However, different properties of dilution gas play important roles on the right branch (when including Ar). As a single-atom gas with a molecular weight of 40, Ar is not similar to O_2 as is N_2. The inclusion of Ar changes the mixture properties, such as the average molecular weight and specific heat capacity ratio, so a rapid decline in R_L appears on the right branch. For cases with more than 3 Ar, the effects of adding more dilution are weaker, and R_L hence approaches a constant.

4. Concluding remarks

To deepen our understanding of the effects of different mixtures, this study simulates ODWs in H_2-O_2-Ar, and the structures are analyzed through comparisons

with ODWs in H_2-O_2-N_2 mixtures. The structures vary with different M_0, but surprisingly, the structures are also sensitive to P_0 in $2H_2$+O_2+7Ar mixtures. Based on flow field analysis, the ratio of induction and heat release zone lengths, R_L, is proposed to model the difference induced by dilution gas. Generally, R_L is large in N_2 diluted mixtures but small in Ar diluted mixtures. We discuss why low R_L results in pressure-sensitive structures, and R_L is analyzed by adjusting dilution type and ratio. When the dilution gas changes gradually from Ar to N_2, R_L increases slowly first and then declines rapidly to approach a constant. The variation rule of R_L is analyzed and compared with results from calculations of a constant volume explosion, demonstrating how different dilution gases influence ODW structures.

Acknowledgment:

The research is supported by NSFC No. 11822202 and 91641130.

Appendix A

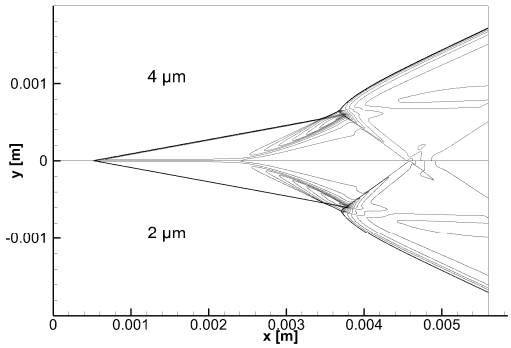

Fig. a1 Density fields with different grid scales in the case of M_0 = 7, P_0 = 1.0 atm.

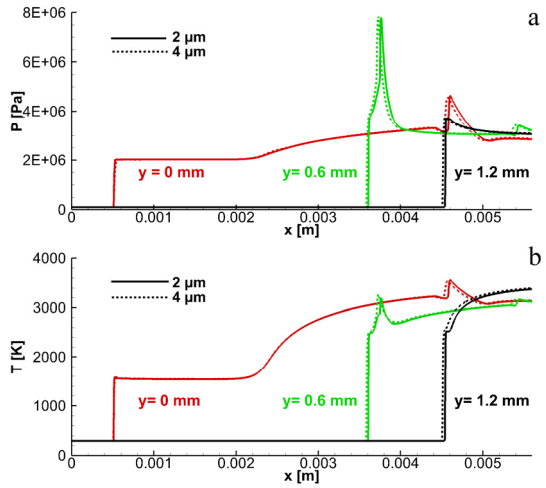

Fig. a2 Pressure and temperature along different x-axis paralleled lines with different grid scales in the case of M_0 = 7, P_0 = 1.0 atm.

Due to several difficulties in experiments, no corresponding experimental results are available to verify the numerical results of ODWs. In several related studies [12, 14], similar structures were observed, and the main problem was whether the grid resolution was sufficient. To examine the effect of grid size, a resolution study was performed here. As shown in Fig. a1, the flow fields are nearly the same with 2 μm and 4 μm grids, and differences are difficult to distinguish. A quantitative comparison is conducted by plotting the pressure and temperature along three typical lines (i.e., y = 0 mm, 0.6 mm, and 1.2 mm) as shown in Fig. a2. These lines correspond to different flow regions on the ODW surface, including oblique shock, near multi-point ODW, and steady ODW. A slight difference is observed, and the curves nearly overlap, so a grid of 4 μm is sufficient to capture the main flow fields. For other cases with different M_0 and P_0, similar resolution studies have been performed to examine and avoid the effects of grid scales.

Appendix B

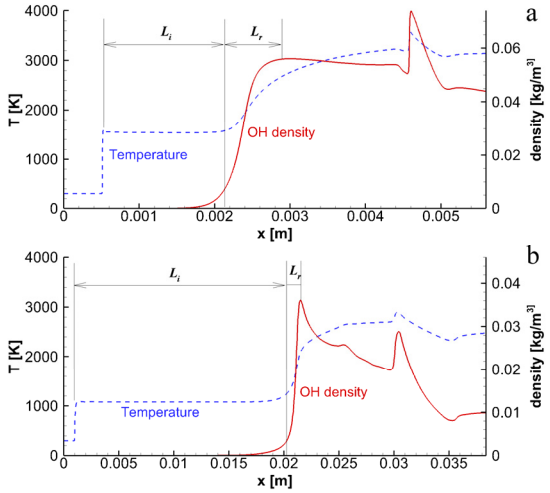

Fig. b1 Temperature and Oh density profiles along the wedge in the case of M_0 = 7, P_0 = 1.0 atm: (a) $2H_2+O_2+7Ar$ and (b) $2H_2+O_2+7N_2$.

The results of detailed chemical reaction models suggest various definitions of induction zone length and heat release zone length. Generally, all parameters with constant values in the induction zone (e.g., pressure, temperature, and density) can be used to define L_i. On the other side, this study uses not only L_i but also L_r, so the unified definition should be considered. In previous studies (e.g., [39]), the temperature and its derivation were used to define L_i and L_r, and the end of the heat release zone may have been underestimated. In this study, after comparing several methods, we chose the density intermediate radical, specie OH, to define the lengths. Generally, OH density is close to 0 in the induction zone but increases to a peak and then declines in the heat release zone.

As shown in Fig. b1, OH density curves are used to define L_i and L_r. The former starts from the shock and ends when clear OH density variation is observed. Compared with the temperature curve, the position is chosen where 15% of the maximum OH density is achieved. This is also the starting point of the heat release zone, which ends at 95% of the maximum OH density. In a few cases, the OH density increases monotonically in the heat release region, but two sections with different slopes can be observed. The ending point of the heat release zone is thus determined by the first-order derivative of OH density to capture the main heat release zone. Based on this method,

results are displayed in Table 2 in the main text. The criteria of length definitions (i.e., 15% and 95%) are not universal, and similar values can be used. As such, the detailed values shown in Table 2 and Fig. 11 may vary, but the conclusions should remain the same.

Reference

[1] Lee JHS. The detonation phenomenon. New York: Cambridge University Press; 2008.

[2] Roy GD, Frolov SM, Borisov AA, Netzer DW. Pulse detonation propulsion: challenges, current status, and future perspective. Prog Energy Combust Sci 2004;30:545-672.

[3] Wolanski P. Detonation propulsion. Proc Combust Inst 2013;34:125-58.

[4] Braun EM, Lu FK, Wilson DR, Camberos JA. Airbreathing rotating detonation wave engine cycle analysis. Aerosp Sci Technol 2013;27:201-8.

[5] Lu FK, Fan H, Wilson DR. Detonation waves induced by a confined wedge. Aerosp Sci Technol 2006;10(8):679-85.

[6] Pratt DT, Humphrey JW, Glenn DE. Morphology of standing oblique detonation waves. J Propul Power 1991;7(5):837-45.

[7] Li C, Kailasanath K, Oran ES. Detonation structures behind oblique shocks. Phys Fluids 1994;4 :1600-11.

[8] Figueira da Silva LF, Deshaies B. Stabilization of an oblique detonation wave by a wedge: a parametric numerical study. Combust Flame 2000;121:152-66.

[9] Teng HH, Jiang ZL. On the transition pattern of the oblique detonation structure. J Fluid Mech 2012;713:659-69.

[10] Zhang Y, Zhou L, Gong J, Ng HD, Teng H. Effects of activation energy on the instability of oblique detonation surfaces with a one-step chemistry model. Phys. Fluids 2018; 30, 106110

[11] Fang Y, Zhang Y, Deng X, Teng H, Numerical study of wedge-induced oblique detonation in acetylene-oxygen- argon mixtures. Phys. Fluids 2019; 31, 026198.

[12] Choi JY, Kim DW, Jeung IS, Ma F, Yang V. Cell-like structure of unstable oblique detonation wave from high-resolution numerical simulation. Proc Combust Inst 2007;31:2473-80.

[13] Verreault J, Higgins AJ, Stowe RA. Formation of transverse waves in oblique detonations. Proc

Combust Inst 2013;34(2):1913-20.

[14] Teng HH, Jiang ZL, Ng HD. Numerical study on unstable surfaces of oblique detonations. J Fluid Mech 2014;744:111-28.

[15] Teng H, Ng HD, Li K, Luo C, Jiang Z. Cellular structure evolution on oblique detonation surfaces. Combust Flame 2015;162:470-7.

[16] Yang P, Ng HD, Teng H, Jiang Z. Initiation structure of oblique detonation waves behind conical shocks. Phys Fluids 2017;29(8):086104.

[17] Ren Z, Wang B, Xiang G, Zheng L. Effect of the multiphase composition in a premixed fuel-air stream on wedge-induced oblique detonation stabilisation. J Fluid Mech 2018;846:411-27.

[18] Miao S, Zhou J, Lin Z, Cai X, Liu S. Numerical study on thermodynamic efficiency and stability of oblique detonation waves. AIAA J 2018;56:3112-22.

[19] Zhang B. The influence of wall roughness on detonation limits in hydrogen-oxygen mixture. Combust Flame 2016;169:333-9.

[20] Zhang B, Liu H. The effects of large scale perturbation-generating obstacles on the propagation of detonation filled with methane-oxygen mixture. Combust Flame 2017;182:279-87.

[21] Zhang B, Liu H, Yan B. Effect of acoustically absorbing wall tubes on the near-limit detonation propagation behaviors in a methane-oxygen mixture. Fuel 2019;236:975-83.

[22] Zhang B, Liu H, Yan B. Investigation on the detonation propagation limit criterion for methane-oxygen mixtures in tubes with different scales. Fuel 2019;239:617-22.

[23] Gutiérrez Marcantoni LF, Tamagno J, Elaskar S. A numerical study on the impact of chemical modeling on simulating methane-air detonations. Fuel 2019; 240:289-298.

[24] Schwer D, Kailasanath K. Fluid dynamics of rotating detonation engines with hydrogen and hydrocarbon fuels. Proc Combust Inst 2013;34:1991-8.

[25] Pan Z, Qi J, Pan J, Zhang P, Zhu Y, Gui M. Fabrication of a helical detonation channel: effect of initial pressure on the detonation propagation modes of ethylene/oxygen mixtures. Combust Flame 2018;192:1-9.

[26] Yang P, Teng H, Ng HD, Z. Jiang, A numerical study on the instability of oblique detonation waves with a two-step induction-reaction kinetic model. Proc Combust Inst 2019;37:3537-44.

[27] Yang P, Teng H, Jiang Z, Ng HD. Effects of inflow Mach number on oblique detonation initiation with a two-step induction-reaction kinetic model. Combust Flame 2018;193:246-56.

[28] Fang Y, Hu Z, Teng H, Jiang Z, Ng HD. Effects of inflow equivalence ratio inhomogeneity on oblique detonation initiation in hydrogen-air mixtures. Aerosp Sci Technol 2017;71:256-63.

[29] Iwata K, Nakaya S, Tsue M. Wedge-stabilized oblique detonation in an inhomogeneous hydrogen–air mixture. Proc Combust Inst 2017;36(2):2761-9.

[30] Teng H, Ng HD, Jiang Z. Initiation characteristics of wedge-induced oblique detonation wave in a stoichiometric hydrogen-air mixture. Proc Combust Inst 2017;36(2):2735-42.

[31] Fang Y, Hu Z, Teng H. Numerical investigation of oblique detonations induced by a finite wedge in a stoichiometric hydrogen-air mixture. Fuel 2018;234:502-07.

[32] Lee JHS. Dynamic parameters of gaseous detonations. Ann Rev Fluid Mech 1984;16:311-36.

[33] Hu XY, Zhang DL, Khoo BC, Jiang ZL. The structure and evolution of a two-dimensional H_2/O_2/Ar cellular detonation. Shock Waves 2004;14(1):37-44.

[34] Taylor BD, Kessler DA, Gamezo VN, Oran ES. Numerical simulations of hydrogen detonations with detailed chemical kinetics. Proc Combust Inst 2013;34:2009–16.

[35] Burke MP, Chaos M, Ju Y, Dryer FL, Klippenstein SL. Comprehensive H_2/O_2 kinetic model for high-pressure combustion. Int J Chem Kinetics 2012;44(7):444-74.

[36] McBride JM, Zehe JZ, Gordon S. NASA Glenn coefficients for calculating thermodynamic properties of individual species. NASA/TP-2002-211556.

[37] Jiang Z. On dispersion-controlled principles for non-oscillatory shock-capturing schemes. Acta Mech Sin 2004;20 (1):1-15 .

[38] Yee HC, Kotov DV, Wang W, Shu CW. Spurious behavior of shock-capturing methods by the fractional step approach: problems containing stiff source terms and discontinuities. J Comp Phys 2013;241:266-91.

[39] Ng HD, Radulescu MI, Higgins AJ, et al. Numerical investigation of the instability for one-dimensional Chapman–Jouguet detonations with chain-branching kinetics. Combustion Theory and Modelling 2005;9(3):385-401.

[40] Kee RJ, Rupley FM, Meeks E, Miller JA. CHEMKIN-III: a fortran chemical kinetic package for the anaylsis of gas-phase chemical and plasma knietics, Report No. SAND-96-8216, Sandia National Labs, Livermore, CA , USA, 1996.